Magazine of Civil Engineering

ISSN 2712-8172

journal homepage: http://engstroy.spbstu.ru/

Research article

UDC 624.04

DOI: 10.34910/MCE.128.2

The beam finite element with five nodal degrees of freedom

Yu.Ya. Tyukalov ✉

Vyatka State University, Kirov, Russian Federation

✉ *yutvgu@mail.ru*

Keywords: finite element, five degrees of freedom, reinforced concrete beam, physical nonlinearity, deformation, axis curvature, failure load

Abstract. The article presents comparative calculations of reinforced concrete beams using two types of beam finite elements: with three and five nodal degrees of freedom. Calculations were performed both taking into account the concrete and reinforcement physical nonlinearity, and without taking it into account. The expressions for stiffness matrix elements and the load vector were obtained for the finite element with five nodal degrees of freedom. Calculations taking into account physical nonlinearity were performed using the variable elasticity parameters method. As a structure for comparing solutions obtained by the two types of finite elements, a single-span clamped horizontal and inclined reinforced concrete beam were used. The accuracy of calculating beam axis deformations and curvature depending on the number and type of finite elements was assessed. It was shown that when performing linear calculations, bending moments, longitudinal forces and displacements do not depend on the number of finite elements with five degrees of freedom into which the beam had been divided. When solving physically nonlinear problems, if we refine the finite element mesh, the solutions obtained for elements with three degrees of freedom tend to the solutions obtained for a smaller number of elements with five degrees of freedom. The proposed beam finite element with five nodal degrees of freedom makes it possible to determine more accurately the axis curvature and deformation, which is especially important when solving physically nonlinear problems.

Citation: Tyukalov, Yu.Ya. The beam finite element with five degrees of node's freedoms. Magazine of Civil Engineering. 2024. 17(4). Article no. 12802. DOI: 10.34910/MCE.128.2

1. Introduction

The bending beams, compressed-bending and tensile rods are widely used in the building structures for various purposes. A large number of scientific articles are devoted to the use of finite element method (FEM) for calculation of such structures.

In [1], to calculate the beams on an elastic foundation, a finite element with three degrees of freedom at the nodes was used. The article notes the simplicity of the mathematical apparatus and the clarity of the diagram, which make the simplified FEM under consideration very flexible and allow us to solve the basic problems of calculating beams on an elastic foundation and other problems.

Article [2] is devoted to the three-dimensional nonlinear finite element analysis of inflatable beams. The beams under consideration are made of modern textile materials and, when inflated, can be used as load-bearing beams or arches. A three-noded spatial element was used, which has five degrees of each node freedom: an axial displacement along the beam element local axis, two transverse displacements along the two main axes, and two rotation angles. It was shown that the beam models had been in good agreement with the nonlinear thin-shell model.

In [3], the study develops a finite element formulation for the distortional buckling of I-beams. The formulation characterizes the distribution of the lateral displacement along the web height by superposing (a) two linear modes intended to capture classical non-distortional lateral-torsional behavior and (b) any

© Tyukalov, Yu.Ya., 2024. Published by Peter the Great St. Petersburg Polytechnic University.

number of user-specified Fourier terms intended to capture additional web distortion. All displacement fields characterizing the lateral displacements are taken to follow a cubic distribution in the longitudinal direction.

Currently, volumetric finite elements are often used to study reinforced concrete bars. In [4, 5], a reinforced concrete beam is modeled using volumetric finite elements, taking into account the possible slipping of reinforcing bars and fibers. Based on the results of the study, recommendations were made on the reinforcement anchorage length.

In [6], a curved beam three-node finite element with nine degrees of freedom at each node was used to model multilayer beams with an arbitrary cross-section. It was noted that the numerical results indicate the effectiveness of the proposed contact solution to problems entailing various contact configurations.

Article [7] presents the formulation of strain-based finite elements for modelling composite beams with finger joints considering slip between the layers. The finite elements were derived in accordance with Reissner beam theory based on the modified virtual work principle where the displacements and rotations had been eliminated from the problem and axial deformation, shear deformation and curvature of the layers remain only functions to be approximated within the finite element. It was noted that the numerical model had been thoroughly tested and the results had shown that the presented finite element formulation had been an efficient tool for practical calculations.

Article [8] was devoted to the modeling of the nonlinear behavior of reinforced concrete structures subject to transverse shear or torsion under monotonic and cyclic loading. The fiber beam element approach was improved for shear effects. The 3D beam element was improved by adding an additional degree of freedom, which represented the deformation displacements of the cross-section. The element formulation was verified using an analytical solution for transverse shear, and 3D simulations of beams subject to shear and torsion.

Article [9] presents a new finite element formulation for the nonlinear analysis of two-layer composite planar frames with an interlayer slip. For each layer the geometrically nonlinear Reissner beam theory was assumed. As shown in one of the numerical examples, the use of the geometrically linear theory instead of the nonlinear one can lead to an error in determining the axial forces and bending moments in each layer as big as 20–80 %.

To calculate reinforced concrete and steel concrete beams taking into account physical nonlinearity, volumetric finite elements are often used [10–13]. A simply supported concrete fiber-reinforced beam was modeled using nonlinear volumetric eight-node finite elements in [10]. The work made an important conclusion: the presence of some fiber type in mortars can reduce compressive and flexural strength. This can be attributed to several factors: a decrease in the density of specimens, weak interfacial adhesion and negatively affected cement hydration, etc.

The principal purpose of [14] was to compare three different ways of determination of critical moment, also in the context of structural sensitivity analysis with respect to the structural element length. Sensitivity gradients were determined using the analytical solution, the finite difference and the finite element methods. The most important conclusion drawn from the computational analysis carried out in this paper was good agreement of all available methods, i.e., analytical methods, finite difference, and finite element methods, to determine the critical moment in thin-walled single-span structures.

Article [15] presents numerical and experimental studies of T-shaped reinforced concrete beams.

The various finite elements types were used to model the performance of box girder bridges [16–18]. Article [16] formulated a novel one-dimensional refined beam FEM that takes into account non-uniform distortional warping and secondary distortional moment deformation effect to analyze the deformation of thin-walled multi-cell box beams. This finite element was based on an extended version of generalized Vlasov's thin-walled beam theory. The proposed one-dimensional beam elements demonstrated desirable predictions for the deformation behavior of thin-walled single- or multi-cell box beams with constant or variable depth. The accuracy and reliability of these predictions were compared to shell finite element calculations.

Article [19] for the multilayer beams analysis proposes a finite element based on nonlinear Reissner beam theory. The connection between the layers was specified by an arbitrary function of the stiffness of springs, continuously distributed along the element length. The displacement field on which the stiffness function depends upon was expressed in a local, deformed basis. The large movements and rotations were taken into account. Distributed force which resulted from the interaction between layers, was included in the governing equations to avoid the need for additional interface elements and to integrate the equations using a single numerical method. The predicted deflection curve of each beam was compared to its experimental counterpart over the entire load range up to failure, and the two curves were found to be in reasonable agreement. A distinctive feature of the present analysis is that it captures not only the onset

and propagation of the delamination process, but also the total post-peak load or softening response of each beam.

Article [20] studied beam finite elements that use absolute nodal coordinates to express deformations. Such finite elements use strain gradient components rather than rotational degrees of freedom, resulting in a consistent and constant mass matrix. The article noted that most of the considered methods for eliminating locking gave the expected results compared to classical finite elements.

Article [21] presented a method for determining all six stress components for a cantilever-type beam that was subjected to concentrated end loads. The method considered an inhomogeneous cross-section and used the cylindrically orthotropic properties of the material. The solution was based on a displacement field formulation that includes unknown in-plane distortion and warping functions. A simple FEM procedure was then used. The efficacy of the method was confirmed by a series of numerical examples corresponding to the analytical results.

Article [22] addresses contact problems associated with large deformations of curved beams. Noted, the contact was difficult to analyze due to uncertainty of the contact positions and strong nonlinearity. A new adaptive differential quadrature element method was proposed to predict the contact positions of a curved beam with a finite number of contact points. The simulation results showed that the proposed element method significantly improved the efficiency and accuracy of solving the curved beam large-deformation contact problem.

Article [23] proposes a general procedure of actions aimed at increasing the seismic resistance of the foundations of turbine units. Implementation of the proposed methodology was carried out on a specific example of a vibroisolated foundation: the dependences of seismic accelerations and displacements were obtained for different variants of seismic isolation.

The beam finite elements are often used for the analysis of various multilayer's types [24–26] and multi-stage beams [27]. Article [24] presents a beam finite element for modal analysis of a double symmetric cross-section made of a functionally graded material. The material properties in a real beam can vary continuously in longitudinal direction, while the variation with respect to the transversal and lateral directions was assumed to be symmetric in a continuous or discontinuous manner. The influence of shear force deformation was taken into account, as well as the influence of longitudinally varying inertia and rotational inertia.

Article [28] aims to study the influences of the viscoelastic and anisotropic properties of a material on the dynamical behavior of the plate. For the first time, an integral model is used to consider the viscoelastic properties of materials of an anisotropic structure. The integral mode correctly describes the rheological processes occurring in the studied structure during the entire time. The presented mathematical model makes it possible to obtain sufficiently accurate solutions that are well combined with experimental results.

Articles [29–31] presented finite elements constructed based on the stress's approximations. The solutions were based on the additional energy functional, to which algebraic equilibrium equations were added using Lagrange multipliers. The stresses or forces can be approximated over the finite element domain by constant or piecewise constant functions. In [32], a beam finite element with five degrees of freedom was proposed to solve problems of beam systems stability. A deformation and axis curvature were added to the standard nodal degrees of freedom. These works show that such finite element makes it possible to more accurately determine critical forces with minimum finite elements number.

A number of works present beam finite elements for the calculation of composite steel-concrete [33] and wood, in combination with a steel profile [34], structures. In papers, the comparison of solutions with experimental results was presented. The finite elemental analysis was also used for the design of laminated timber beams [35, 36]. The works examine the bending and shear stiffness of wooden beams with a composite cross-section. The tests of wooden samples and beams were carried out. A comparison was made between the experimental data and the finite element analysis results.

The purpose of current work is to perform comparative calculations of reinforced concrete beams using beam finite elements of two types: with three and five degrees of freedom at the node. The calculations must be performed both taking into account the physical nonlinearity of concrete and reinforcement, and without taking it into account. It assumes to evaluate the accuracy of calculating deformations and curvature of the beam axis depending on the number and finite elements type, as well as the accuracy of calculating stresses in reinforcing bars in the process of increasing the load until failure.

2. Methods

When solving structural mechanics problems using FEM, taking into account physical nonlinearity, the importance of determining deformations accuracy in the finite element region increases. The more accurately the deformations are calculated, the more accurately the stiffness finite elements parameters will be determined, and the more accurately the stresses and displacements will be determined.

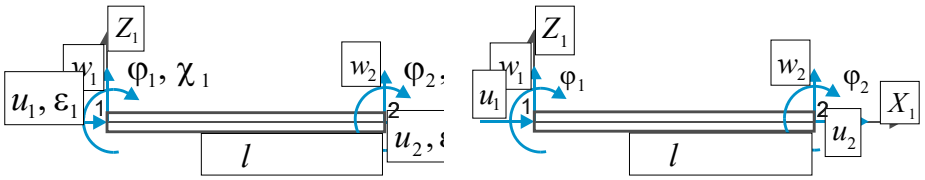

Figure 1. Variants of a rod finite element nodal unknowns.

In the standard rod finite element (Fig. 1a), the following polynomials are used to approximate the displacement fields:

$$
\begin{aligned}
&w(x)=N_1(x)w_1+N_2(x)\varphi_1+N_3(x)w_2+N_4(x)\varphi_2;\\
&u(x)=N_5(x)u_1+N_6(x)u_2;\\
&N_1(x)=1+2(x/l)^3-3(x/l)^2,\quad N_3(x)=3(x/l)^2-2(x/l)^3;\\
&N_2(x)=-x\left[(x/l)-1\right]^2,\quad N_4(x)=-x\left[(x/l)^2-x/l\right];\\
&N_5(x)=1-x/l,\quad N_6(x)=x/l.
\end{aligned}
\tag{1}
$$

The deformations at any point in the finite element cross-section are determined by the deformation of the neutral axis ε_0 and the axis curvature value χ_0:

$$
\begin{aligned}
&\varepsilon_0(x)=\frac{du}{dx}=(-u_1+u_2)/l;\\
&\chi_0(x)=\frac{d^2w}{dx^2}=\frac{6}{l^2}\left[(2x/l)-1\right]w_1-\frac{2}{l}\left[(3x/l)-2\right]\varphi_1-\\
&\quad-\frac{6}{l^2}\left[(2x/l)-1\right]w_2-\frac{2}{l}\left[(3x/l)-1\right]\varphi_2.
\end{aligned}
\tag{2}
$$

Thus, the neutral axis deformations are constant along the finite element length, and the axis curvature changes linearly. The axis curvature value at the beginning or end of an element depends on the displacement and rotation angle of the opposite node. Therefore, it is obvious that during the transition from one finite element to another, at the nodal point the deformations can undergo a discontinuity, both due to a jump in the axis deformation ε_0 and due to a discontinuity in the axis curvature value χ_0. Below we will give numerical examples illustrating discontinuities in the deformation fields at the nodal points of the finite element mesh.

In [32], to solve rod systems stability problems, a finite element with five degrees of nodal freedom was proposed (Fig. 1b). To approximate transverse displacements a fifth-degree polynomial was used, and for longitudinal displacements a third-degree polynomial was used. The deformation of the neutral axis and curvature were taken as additional unknowns at the nodes. Thus, if necessary, the deformations continuity at nodal points is ensured.

The functions of a finite element transverse and longitudinal displacements are determined by expressions (3–5):

$$
\begin{aligned}
&w(x)=H_1(x)w_1+H_2(x)\varphi_1+H_3(x)\chi_1+H_4(x)w_2+H_5(x)\varphi_2+H_6(x)\chi_2;\\
&u(x)=H_7(x)u_1+H_8(x)\varepsilon_1+H_9(x)u_2+H_{10}(x)\varepsilon_2.
\end{aligned}
\tag{3}
$$

$$
\begin{aligned}
H_1(x) &= 1-10(x/l)^3+15(x/l)^4-6(x/l)^5;\\
H_2(x) &= l\left[x/l-6(x/l)^3+8(x/l)^4-3(x/l)^5\right];\\
H_3(x) &= \frac{l^2}{2}\left[(x/l)^2-3(x/l)^3+3(x/l)^4-(x/l)^5\right];\\
H_4(x) &= 10(x/l)^3-15(x/l)^4+6(x/l)^5;\\
H_5(x) &= l\left[-4(x/l)^3+7(x/l)^4-3(x/l)^5\right];\\
H_6(x) &= \frac{l^2}{2}\left[(x/l)^3-2(x/l)^4+(x/l)^5\right].
\end{aligned}
\tag{4}
$$

$$
\begin{aligned}
H_7(x) &= 1-3(x/l)^2+2(x/l)^3;\\
H_8(x) &= l\left[x/l-2(x/l)^2+(x/l)^3\right];\\
H_9(x) &= 3(x/l)^2-2(x/l)^3;\\
H_{10}(x) &= l\left[-(x/l)^2+(x/l)^3\right].
\end{aligned}
\tag{5}
$$

In this case, the neutral axis deformation varies along its length as a quadratic function, and the axis curvature varies according to a cubic polynomial:

$$
\begin{aligned}
\varepsilon_0(x) = \frac{du}{dx} = \frac{6}{l}\left[-(x/l)+(x/l)^2\right]u_1+\left[3(x/l)^2-4(x/l)+1\right]\varepsilon_1+\\
+\frac{6}{l}\left[(x/l)-(x/l)^2\right]u_2+\left[3(x/l)^2-2(x/l)\right]\varepsilon_2.
\end{aligned}
\tag{6}
$$

$$
\begin{aligned}
\chi_0(x) = \frac{d^2w}{dx^2} = \frac{60}{l^2}\left[-(x/l)+3(x/l)^2-2(x/l)^3\right]w_1+\\
+\frac{12}{l}\left[-3(x/l)+8(x/l)^2-5(x/l)^3\right]\varphi_1+\left[1-9(x/l)+18(x/l)^2-10(x/l)^3\right]\chi_1+\\
+\frac{60}{l^2}\left[(x/l)-3(x/l)^2+2(x/l)^3\right]w_2+\frac{12}{l}\left[-2(x/l)+7(x/l)^2-5(x/l)^3\right]\varphi_2+\\
+\left[3(x/l)-12(x/l)^2+10(x/l)^3\right]\chi_2.
\end{aligned}
\tag{7}
$$

In the future, we will agree to denote a finite element with three degrees of freedom as FE-3, and with five degrees of freedom as FE-5.

Let us obtain expressions for the secant stiffness matrix's elements of a reinforced concrete finite element, the cross section of which is shown in Fig. 2. A concrete and reinforcement can have arbitrary nonlinear dependencies $\sigma(\varepsilon)$. The number of reinforcement layers in a section is also arbitrary.

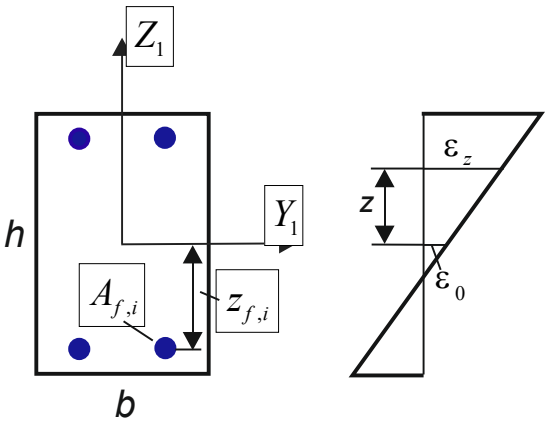

Figure 2. The beam cross section and deformations diagram.

$A_{f,i}$ is reinforcing bar cross-sectional area; $z_{f,i}$ is coordinate of the reinforcing bar position along Z_1 the axis; b, h are cross-sectional dimensions. We write the expressions for the median plane deformations and the axis curvature in the following vector form:

$$\varepsilon_0 = \mathbf{N}_{\mathrm{u}}^{\mathrm{T}}\mathbf{z}_{\mathrm{u}}, \quad \chi_0 = \mathbf{N}_{\mathrm{w}}^{\mathrm{T}}\mathbf{z}_{\mathrm{w}}. \tag{8}$$

For FE-3 with three nodal degrees of freedom, we obtain the following expressions:

$$\begin{aligned} \mathbf{N}_{\mathrm{u}}^{\mathrm{T}} &= \left[N_5'(x) \quad N_6'(x)\right]; \\ \mathbf{N}_{\mathrm{u}}^{\mathrm{T}} &= \left[N_1''(x) \quad N_2''(x) \quad N_3''(x) \quad N_4''(x)\right]. \end{aligned} \tag{9}$$

$$\mathbf{z}_{\mathrm{u}} = \begin{bmatrix} u_1 \\ u_2 \end{bmatrix}, \quad \mathbf{z}_{\mathrm{w}} = \begin{bmatrix} w_1 \\ \varphi_1 \\ w_2 \\ \varphi_2 \end{bmatrix}. \tag{10}$$

For FE-5 with five nodal degrees of freedom, the expressions will be as follows:

$$\begin{aligned} \mathbf{N}_{\mathrm{u}}^{\mathrm{T}} &= \left[N_7'(x) \quad N_8'(x) \quad N_9'(x) \quad N_{10}'(x)\right]; \\ \mathbf{N}_{\mathrm{u}}^{\mathrm{T}} &= \left[N_1''(x) \quad N_2''(x) \quad N_3''(x) \quad N_4''(x) \quad N_5''(x) \quad N_6''(x)\right]. \end{aligned} \tag{11}$$

$$\mathbf{z}_{\mathrm{u}} = \begin{bmatrix} u_1 \\ \varepsilon_1 \\ u_2 \\ \varepsilon_2 \end{bmatrix}, \quad \mathbf{z}_{\mathrm{w}} = \begin{bmatrix} w_1 \\ \varphi_1 \\ \chi_1 \\ w_2 \\ \varphi_2 \\ \chi_2 \end{bmatrix}. \tag{12}$$

Using the above notations, the strain energy expression of the finite element will have the following form:

$$E = \frac{1}{2}\int_{-h/2}^{h/2}\int_0^l bE_b^s\left(\varepsilon_0 - z\chi_0\right)^2 dxdz + \frac{1}{2}\sum_{i=1}^{n_f}\int_0^i E_{f,i}^s A_{f,i}\left(\varepsilon_0 - z_{f,i}\chi_0\right)^2 dx. \tag{13}$$

We take denotations for the cross-section rigidity parameters:

$$EI(x)=\int_{-h/2}^{h/2} z^2 bE_b^s dz+\sum_{i=1}^{n_f} E_f^s A_{f,i} z_{f,i}^2;$$

$$EA(x)=\int_{-h/2}^{h/2} bE_b^s dz+\sum_{i=1}^{n_f} E_f^s A_{f,i}; \tag{14}$$

$$ES(x)=\int_{-h/2}^{h/2} zbE_b^s dz+\sum_{i=1}^{n_f} E_f^s A_{f,i} z_{f,i}.$$

The expression (13) can be written in the following form:

$$E=\frac{1}{2}\int_0^l \left(EA(x)\varepsilon_0^2+EI(x)\chi_0^2-2ES(x)\varepsilon_0\chi_0 \right) dx. \tag{15}$$

Substituting (8) into (15), we get:

$$\begin{aligned} E=\frac{1}{2}\int_0^l \Big(& EI(x)\mathbf{z}_{\mathrm{w}}^{\mathrm{T}}\mathbf{N}_{\mathrm{w}}\mathbf{N}_{\mathrm{w}}^{\mathrm{T}}\mathbf{z}_{\mathrm{w}}+EA(x)\mathbf{z}_{\mathrm{u}}^{\mathrm{T}}\mathbf{N}_{\mathrm{u}}\mathbf{N}_{\mathrm{u}}^{\mathrm{T}}\mathbf{z}_{\mathrm{u}}- \\ & -ES(x)\mathbf{z}_{\mathrm{w}}^{\mathrm{T}}\mathbf{N}_{\mathrm{w}}\mathbf{N}_{\mathrm{u}}^{\mathrm{T}}\mathbf{z}_{\mathrm{u}}-ES(x)\mathbf{N}_{\mathrm{u}}^{\mathrm{T}}\mathbf{z}_{\mathrm{u}}\mathbf{N}_{\mathrm{w}}^{\mathrm{T}}\mathbf{z}_{\mathrm{w}} \Big) dx. \end{aligned} \tag{16}$$

Let us introduce the following notation:

$$\begin{gathered} \mathbf{K}_{\mathrm{ww}}=\int_0^l EI(x)\mathbf{N}_{\mathrm{w}}\mathbf{N}_{\mathrm{w}}^{\mathrm{T}}dx, \quad \mathbf{K}_{\mathrm{uu}}=\int_0^l EA(x)\mathbf{N}_{\mathrm{u}}\mathbf{N}_{\mathrm{u}}^{\mathrm{T}}dx, \\ \mathbf{K}_{\mathrm{uv}}=-\int_0^l ES(x)\mathbf{N}_{\mathrm{u}}\mathbf{N}_{\mathrm{w}}^{\mathrm{T}}dx. \end{gathered} \tag{17}$$

The finite element stiffness matrix in the local coordinate system will have the following simple form:

$$\mathbf{K}_{\mathrm{L}}=\begin{bmatrix} \mathbf{K}_{\mathrm{ww}} & \mathbf{K}_{\mathrm{uv}}^{\mathrm{T}} \\ \mathbf{K}_{\mathrm{uv}} & \mathbf{K}_{\mathrm{uu}} \end{bmatrix}. \tag{18}$$

For FE-5, the integrals (17) expressions will include the products of the third- and fifth-degrees polynomials. The stiffness parameters (14) for nonlinear problems will be variable along the length of the element. To calculate integrals (17), we apply the well-known Gauss-Legendre numerical integration procedure:

$$\mathbf{K}_{\mathrm{ww}}=\frac{l}{2}\sum_{i=1}^{n_g} G_i EI(x_i)\mathbf{N}_{\mathrm{w}}(x_i)\mathbf{N}_{\mathrm{w}}^{\mathrm{T}}(x_i);$$

$$\mathbf{K}_{\mathrm{uu}}=\frac{l}{2}\sum_{i=1}^{n_g} G_i EA(x_i)\mathbf{N}_{\mathrm{u}}(x_i)\mathbf{N}_{\mathrm{u}}^{\mathrm{T}}(x_i); \tag{19}$$

$$\mathbf{K}_{\mathrm{uv}}=\frac{l}{2}\sum_{i=1}^{n_g} G_i ES(x_i)\mathbf{N}_{\mathrm{u}}(x_i)\mathbf{N}_{\mathrm{w}}^{\mathrm{T}}(x_i), \quad x_i=\frac{l(\xi_i+1)}{2},$$

G_i, ξ_i are weight factor and integration point coordinate on the interval [–1, 1].

To calculate integrals (14) at points x_i corresponding to the Gauss-Legendre coordinates, we use the trapezoidal method:

$$EI\left(x_i\right)=\sum_{k=1}^{n+1} b\Delta h E_b^s z_k^2+\sum_{j=1}^{n_f} E_{f,j}^s A_{f,j} z_{f,j}^2;$$

$$EA\left(x_i\right)=\sum_{k=1}^{n+1} b\Delta h E_b^s+\sum_{j=1}^{n_f} E_{f,j}^s A_{f,j};\tag{20}$$

$$ES\left(x_i\right)=\sum_{k=1}^{n+1} b\Delta h E_b^s z_k+\sum_{j=1}^{n_f} E_{f,j}^s A_{f,j} z_{f,j}.$$

n is the sections number into which the section during numerical integration is divided by height. The elasticity secant modules E_b^s and $E_{f,j}^s$ are determined from specified dependencies $\sigma\left(\varepsilon\right)$ for concrete and reinforcement. In expressions (20), in accordance with the method of trapezoidal, the following parameters are used:

$$z_k=-\frac{h}{2}+\frac{h\left(k-1\right)}{n},\quad \Delta h=\begin{cases} h/2n, & k=1, k=n+1 \\ h/n, & 1<k<n+1 \end{cases}.\tag{21}$$

The stiffness matrix $\mathbf{K}_{\mathrm{L}}$ expression was obtained in the local coordinate system of the finite element X_1Z_1 (Fig. 1). The direction cosine matrices $\mathbf{C}$ for moving to the global coordinate system are given below:

$$\mathbf{C}=\begin{bmatrix} \cos\alpha & 0 & 0 & 0 & \sin\alpha & 0 \\ 0 & 1 & 0 & 0 & 0 & 0 \\ 0 & 0 & \cos\alpha & 0 & 0 & \sin\alpha \\ 0 & 0 & 0 & 1 & 0 & 0 \\ -\sin\alpha & 0 & 0 & 0 & \cos\alpha & 0 \\ 0 & 0 & -\sin\alpha & 0 & 0 & \cos\alpha \end{bmatrix};$$

$$\mathbf{C}=\begin{bmatrix} \cos\alpha & 0 & 0 & 0 & 0 & 0 & \sin\alpha & 0 & 0 & 0 \\ 0 & 1 & 0 & 0 & 0 & 0 & 0 & 0 & 0 & 0 \\ 0 & 0 & 1 & 0 & 0 & 0 & 0 & 0 & 0 & 0 \\ 0 & 0 & 0 & \cos\alpha & 0 & 0 & 0 & 0 & \sin\alpha & 0 \\ 0 & 0 & 0 & 0 & 1 & 0 & 0 & 0 & 0 & 0 \\ 0 & 0 & 0 & 0 & 0 & 1 & 0 & 0 & 0 & 0 \\ -\sin\alpha & 0 & 0 & 0 & 0 & 0 & \cos\alpha & 0 & 0 & 0 \\ 0 & 0 & 0 & 0 & 0 & 0 & 0 & 1 & 0 & 0 \\ 0 & 0 & 0 & -\sin\alpha & 0 & 0 & 0 & 0 & \cos\alpha & 0 \\ 0 & 0 & 0 & 0 & 0 & 0 & 0 & 0 & 0 & 1 \end{bmatrix}.\tag{22}$$

$$\cos\alpha=\frac{y_2-y_1}{l}.\tag{23}$$

y_1, y_2 are coordinates of the finite element start and end in the global coordinate system. Using (22), we obtain the stiffness matrix $\mathbf{K}_i$ expression for finite element i in the global coordinate system:

$$\mathbf{K}_i=\mathbf{C}^{\mathrm{T}}\mathbf{K}_{\mathrm{L}}\mathbf{C}.\tag{24}$$

Let us calculate the nodal forces vector from the action of uniformly distributed loads on FE-5 in the local coordinate system. The work of distributed loads will be expressed as follows:

$$A_q = \int_0^l \left[q_{z1} w(x) + q_{x1} u(x) \right] dx. \tag{25}$$

$$q_{z1} = q_z \cos\alpha - q_x \sin\alpha, \quad q_{x1} = q_z \sin\alpha + q_x \cos\alpha. \tag{26}$$

Substituting expressions (3–4) into (25), we will obtain:

$$A_q = \mathbf{z}_L^T \mathbf{B}_L, \quad \mathbf{z}_L = \begin{Bmatrix} \mathbf{z}_w \\ \mathbf{z}_u \end{Bmatrix};$$
$$\mathbf{B}_L^T = \left[\frac{q_{z_1} l}{2} \; \frac{q_{z_1} l^2}{10} \; \frac{q_{z_1} l^3}{120} \; \frac{q_{z_1} l}{2} \; \frac{-q_{z_1} l^2}{10} \; \frac{q_{z_1} l^3}{120} \; \frac{q_{x_1} l}{2} \; \frac{q_{x_1} l^2}{12} \; \frac{q_{x_1} l}{2} \; \frac{-q_{x_1} l^2}{12} \right]. \tag{27}$$

Vector $\mathbf{z}_L = \mathbf{C}^T \mathbf{z}$. Then we will get:

$$A_q = \mathbf{z}^T \mathbf{C} \mathbf{B}_L. \tag{28}$$

Calculating the derivative of work (28) with respect to the vector, we obtain the nodal forces vector from the action of uniformly distributed loads in the global coordinate system.

$$\mathbf{R}_q = \mathbf{C} \mathbf{B}_L. \tag{29}$$

For FE-3 vector:

$$\mathbf{B}_L^T = \left[\frac{q_{z_1} l}{2} \; \frac{-q_{z_1} l^2}{12} \; \frac{q_{z_1} l}{2} \; \frac{q_{z_1} l^2}{12} \; \frac{q_{x_1} l}{2} \; \frac{q_{x_1} l}{2} \right]. \tag{30}$$

From the vectors $\mathbf{R}_q$ formed for the finite elements, and the forces and moments concentrated in the nodes, the load vector $\mathbf{R}$ for the entire system is formed. The global stiffness matrix of the system is defined as the sum of finite element stiffness matrices

$$\mathbf{K} = \sum_i \mathbf{K}_i. \tag{31}$$

We write the system of the nonlinear algebraic equations in the following form:

$$\mathbf{K}(\mathbf{Z})\mathbf{Z} = \mathbf{R}. \tag{32}$$

$\mathbf{Z}$ is the nodal unknown's global vector for the entire system.

We will solve the nonlinear equations system (31) using the well-known method of variable elasticity parameters. The main stages of solving the nonlinear problem are presented in Fig. 3.

1. $k = 0, \; \mathbf{Z}_0 = 0$
2. $k = k + 1$
3. $\mathbf{Z}_k = \mathbf{K}^{-1}(\mathbf{Z}_{k-1})\mathbf{R} \pm$
4. $eps = \dfrac{\sum_j \left(Z_{k,j} - Z_{k-1,j} \right)^2}{\sum_j Z_{k,j}^2}$
5. If $eps > 0.005$ then go to 2
6. Exit

Figure 3. The method of elastic solutions algorithm.

3. Results and Discussion

The main aim of this study is to compare the values of curvature and axis deformation for various finite elements sections, obtained when using two options for approximating displacements. As a structure for comparing solutions obtained, using two variants of finite elements FE-3 and FE-5, we will use a single-span clamped horizontal and inclined reinforced concrete beams (Fig. 4). A uniformly distributed vertical load is applied to the beam. In reference sections, both displacements and rotation angles are excluded.

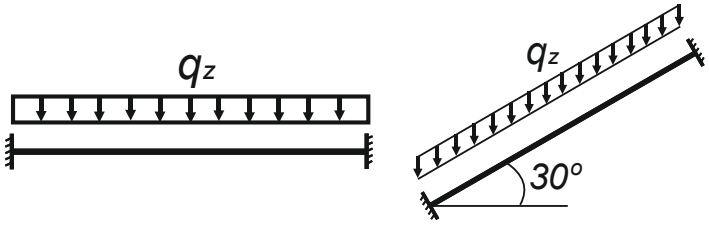

Figure 4. The horizontal and inclined beams.

The beam data are given in Table 1. Stress-strain diagrams for concrete and beam reinforcement are shown in Fig. 5.

Table 1. The clamped beam characteristics.

Beton	Reinforcement	Length, m	b, cm	h, cm	Bottom reinforcement		Top reinforcement	
					Diameter, mm	z_f, mm	Diameter, mm	z_f, mm
B30	A-III	6	20	40	2 d20	– 160	2 d20	160

Tables 2 and 3 present the characteristics of concrete and reinforcement necessary for constructing stress-strain diagrams.

Table 2. The characteristics of concrete.

R_b, MPa	R_{bt}, MPa	ε_{b1}	ε_{b0}	ε_{b2}	ε_{bt1}	ε_{bt0}	ε_{bt2}
17000	1150	– 0.000314	– 0.002	– 0.035	0.0000212	0.0001	0.00015

Table 3. The characteristics of reinforcement.

R_s, MPa	ε_{s0}	ε_{s2}	ε_{st0}	ε_{st2}
350000	– 0.00167	– 0.015	0.00167	0.0015

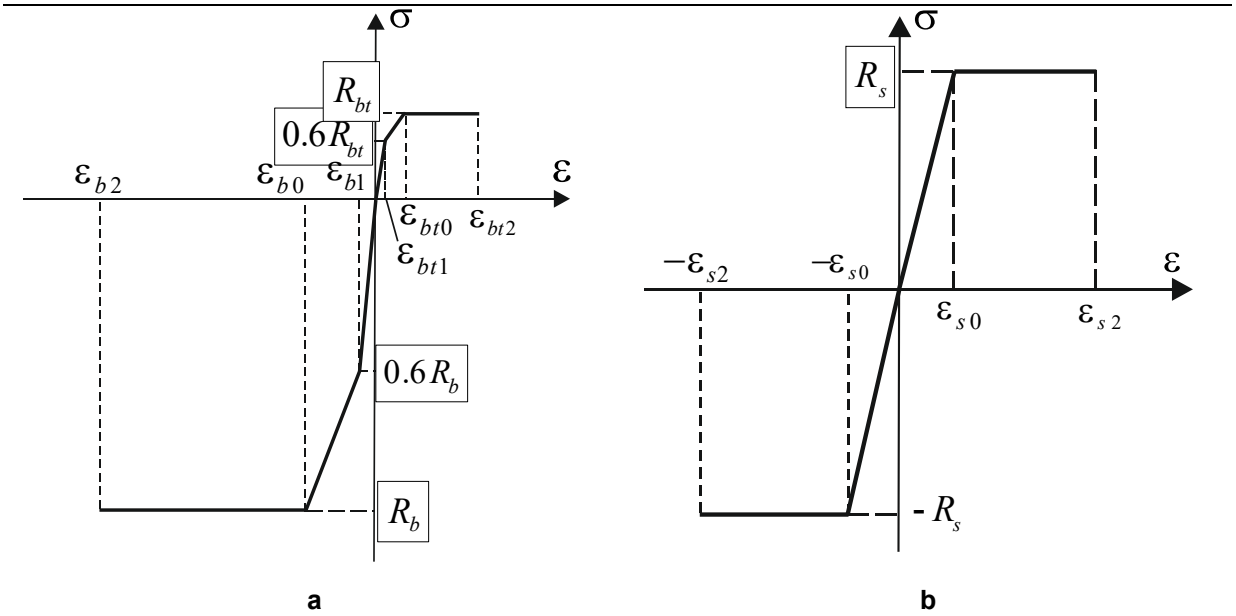

Figure 5. The stress-strain diagrams for concrete and reinforcement.

3.1. Linear Calculations

To compare solutions, beam calculations were performed (Fig. 4) when it was divided along the length into 2, 4, 8 and 16 finite elements. Calculations were performed in a linear formulation at the initial value of the concrete elastic modulus E = 30000 MPa. Reinforcement was not taken into account. The distributed load was assumed to be equal to q = 10 kN/m.

When calculating physically linear problems, it turned out that the bending moments and displacements in all beam nodal sections are the same for both versions of finite elements, regardless of the finite elements number. At the same time, we note that for the FE-5, the solution can also be obtained if the beam is represented by only one finite element. In this case, the only unknown parameters are the beam curvatures at the beginning and end. The solution even with this beam representation was exact.

Table 4. The beam sections axis curvature, q=10 kN/m (Fig. 4a).

A section coordinates along length, m	FE-3 [37]				FE-5	Bending moments, kN·m
	2 elements	4 elements	8 elements	16 elements	1 element	
0	– 0.000578	– 0.0007227	– 0.0007589	– 0.0007679	– 0.0007710	– 30
0.75	– 0.000289	– 0.0002891	– 0.0002530	– 0.0002620	– 0.0002650	– 10.313
1.5	0	0.0001445	0.0001084	0.0000994	0.0000960	3.75
2.25	0.000289	0.0002891	0.0003252	0.0003162	0.0003130	12.188
3.0	0.000578	0.0004336	0.0003975	0.0003885	0.0003850	15

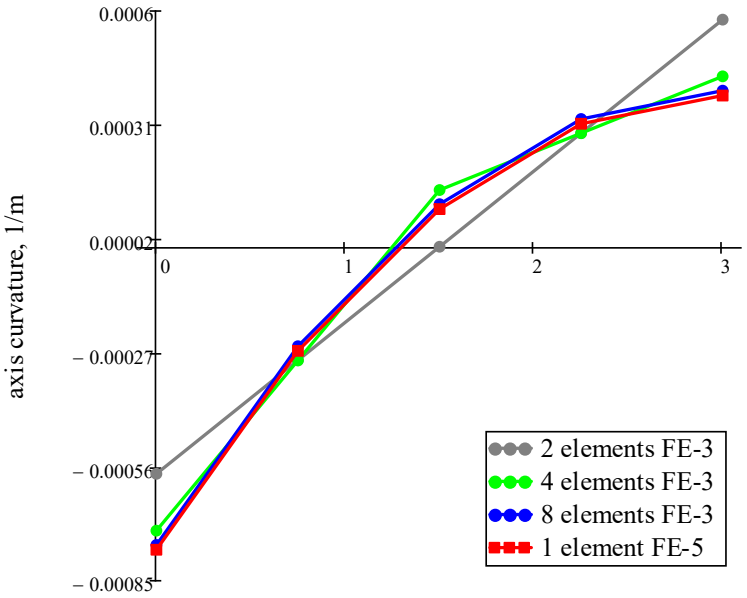

Figure 6. Axis curvature of the clamped beam (Fig. 4a).

Table 4 and Fig. 6 show the axis curvature values for various options for dividing the beam into finite elements under the action of a uniformly distributed load. For FE-5, the curvature values are the same for any elements number. Therefore, Table 4 presents the values for the case of the beam being represented by one FE-5. Using FE-3 [37], calculations were performed when the beam was divided into 2, 4, 8, and 16 finite elements. A comparison of the results shows that when the finite element mesh is refined, the axis curvature values in all beam sections tend to the values, which were obtained for one FE-5. The largest deviation in curvature values is observed in the pinched point. Therefore, when using two FE-3, the curvature value in the pinch point is 25 % less than the value obtained using FE-5. When using four elements, the deviation in this curvature values is 6 %. Therefore, the beam dividing into four FE-3 is not sufficient to obtain accurate curvature values in beam sections. We also note that the use of FE-3 gives underestimated curvature values in the extreme section where the bending moment has a maximum value by module.

Table 5. The vertical displacements of the clamped beam, q=10 kN/m (Fig. 4a).

A section coordinates along length, m	FE-3 [37]			FE-5
	2 elements	4 elements	8 elements	1 element
0	**0**	**0**	**0**	**0**
0.75	– 0.000164	– 0.000197	**– 0.000201**	– 0.000201
1.5	– 0.000525	**– 0.00059**	**– 0.00059**	– 0.00059
2.25	– 0.000885	– 0.000918	**– 0.000922**	– 0.000922
3.0	**– 0.001049**	**– 0.001049**	**– 0.001049**	– 0.001049

Table 5 shows the displacement values of beam sections for various finite element mesh options. The displacement values calculated at the finite element nodes are marked in bold, and the values in intermediate sections located between the finite element nodes are shown in regular font. It is interesting to note that the nodal points displacements when using FE-3 coincide with the values calculated when using one FE-5, and the values at the intermediate points of FE-3 differ from the exact ones.

Thus, for any mesh, the nodal displacements for FE-3 are calculated accurately, and the displacements of intermediate points between nodes approach the exact ones when the mesh is refined. The use of FE-5, due to additional degrees of freedom, leads to the displacement's refinement of intermediate sections between the finite element nodes, as well as to the refinement of axis curvature and deformations at the nodes and in the intermediate sections. In this case, for a clamped beam it is enough to use one FE-5.

Figs. 7–8 show the calculation results of an inclined beam under the uniformly distributed load action (Fig. 4b). In this case, in addition to curvature, longitudinal deformations also occur in the sections.

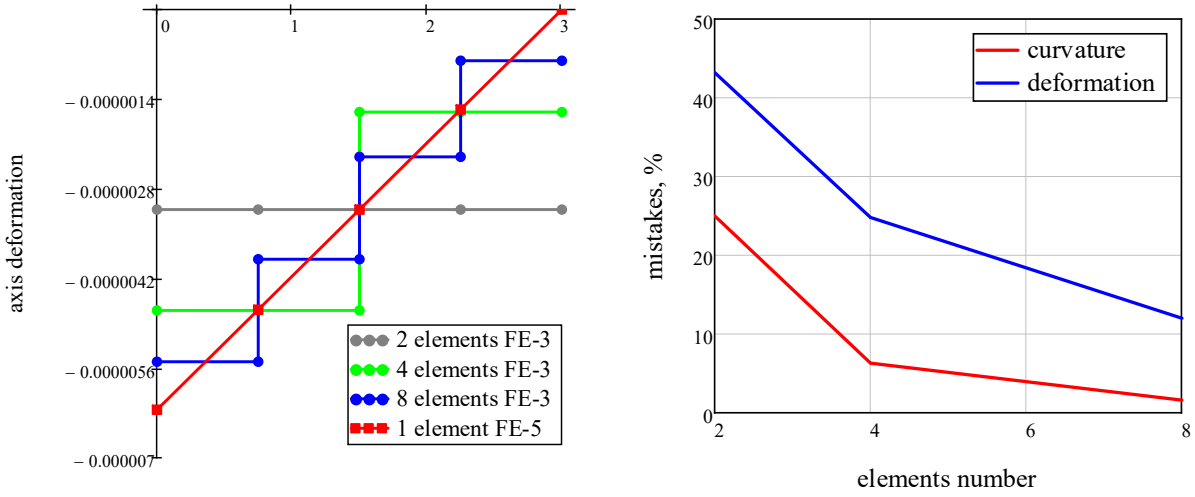

a **b**

Figure 7. The deformations of the inclined clamped beam (Fig. 4b) and errors in calculating curvatures and axis deformations for FE-3.

The graphs of changes in the inclined beam axis curvature, depending on the number and type of finite elements, coincide with the horizontal beam graph (Fig. 6). In this case, compressive forces and, corresponding to them, the beam axis longitudinal deformations arise too (Fig. 7a). When using FE-3, longitudinal deformations change stepwise along the beam length, and when using FE-5, the deformations change linearly, which corresponds to the law of longitudinal forces change. When FE-3 mesh is refined, the longitudinal deformation's values tend to the corresponding values obtained for FE-5. However, even if we use eight FE-3, the error in the longitudinal strains value is more than 10% (Fig. 7b). Fig. 7b also presents the errors in the axis curvature and axis deformation calculation for FE-3 depending on the finite elements number. Note that the error in calculating axis curvature is smaller but also significant when the FE-3 number is small.

3.2. Nonlinear Calculations

To determine the calculating accuracy of the stress-strain state parameters, taking into account the physical nonlinearity of concrete and reinforcement, the calculations were performed for an inclined beam

(Fig. 4b) with symmetrical reinforcement (Fig. 2). The calculations were performed both for different loading levels up to failure, and for different numbers of finite elements FE-3 and FE-5 at the same loading level q_z = 40 kN/m. To guarantee high numerical integration accuracy, during nonlinear calculations the section was divided in height into forty layers and nine Gauss-Legendre integration points were used along the length of the finite element. The nonlinear problem was solved iteratively using the elastic solutions method (Fig. 3). Fig. 8–10 show the calculation results of an inclined reinforced concrete beam (Fig. 4b) on the load action q_z = 40 kN/m.

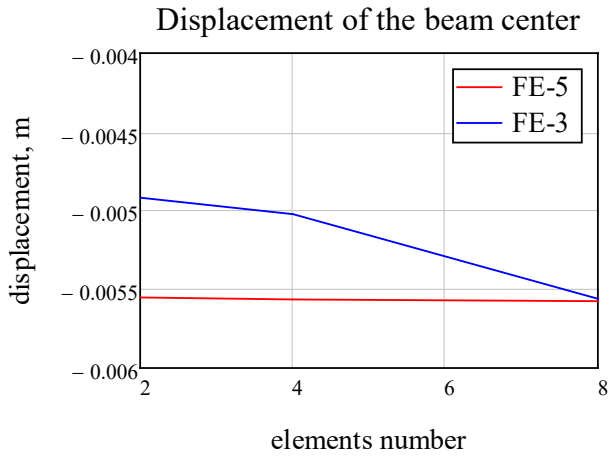

Figure 8. The vertical displacement of the beam center.

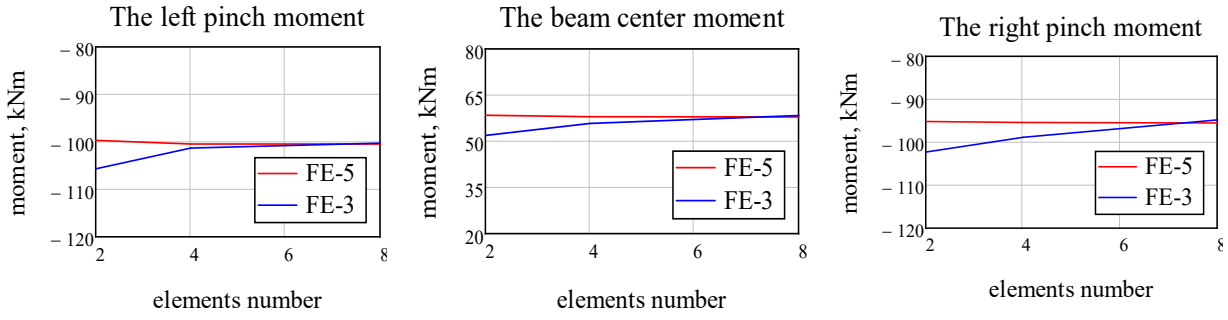

a **b** **c**

Figure 9. The bending moments in the inclined beam at q_z = 40 kN/m.

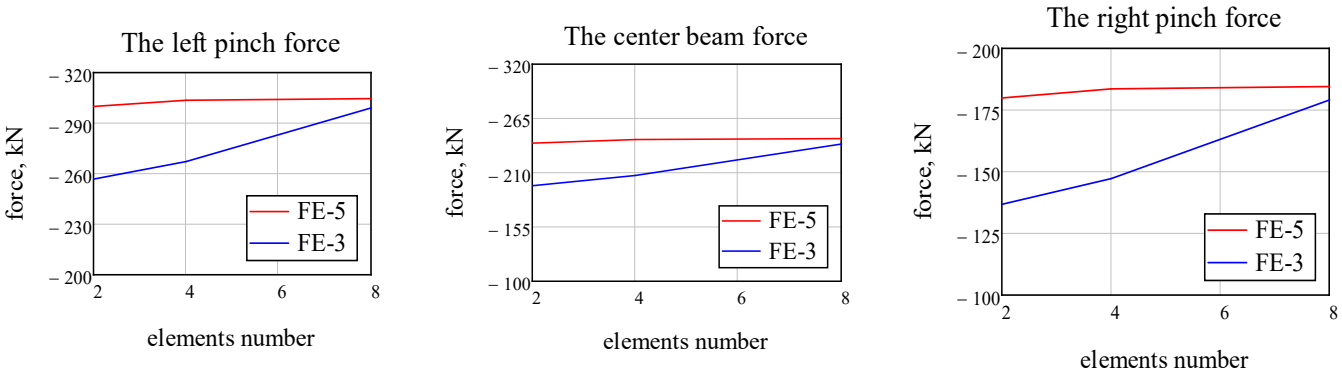

a **b** **c**

Figure 10. The longitudinal forces in the inclined beam at q_z = 40 kN/m.

Comparing the calculation results shown in Fig. 8–10, the following conclusions can be drawn:

- when using FE-5, the displacements magnitude, bending moments and longitudinal forces practically do not depend on the elements number into which the beam is divided;
- when refining the finite element mesh, the solutions obtained for FE-3 tend to the solutions obtained for FE-5;
- the greatest difference between the two solutions is observed for the longitudinal forces magnitudes; for a more accurate longitudinal forces calculation using FE-3, a mesh of at least eight elements is required;
- in contrast to the linear calculation, there is no coincidence of bending moments and displacements at nodal points obtained using finite elements FE-5 and FE-3;
- with four finite elements mesh, the differences in the bending moments values do not exceed 5 %, and for longitudinal forces they can be more than 15 %.

Next, we compare the reinforcing bars stress values. Fig. 11–13 show the reinforcing bars stress values for the support sections and the center of the inclined reinforced concrete beam for various options for beam dividing on the finite elements under the load action. It should be noted that the reinforcement stresses obtained for finite elements FE-3 and FE-5 differ more significantly, compared to the difference of the bending moments and longitudinal forces values. Bending moments and longitudinal forces differ little with the eight finite elements mesh, and the stresses in tensile reinforcement of the left and right support sections, in this case, differ by 27–28 % (Table 6). These calculation results are consistent with the results obtained from linear calculations, which showed that when we use FE-3, deformations and curvatures are calculated less accurately than moments and longitudinal forces.

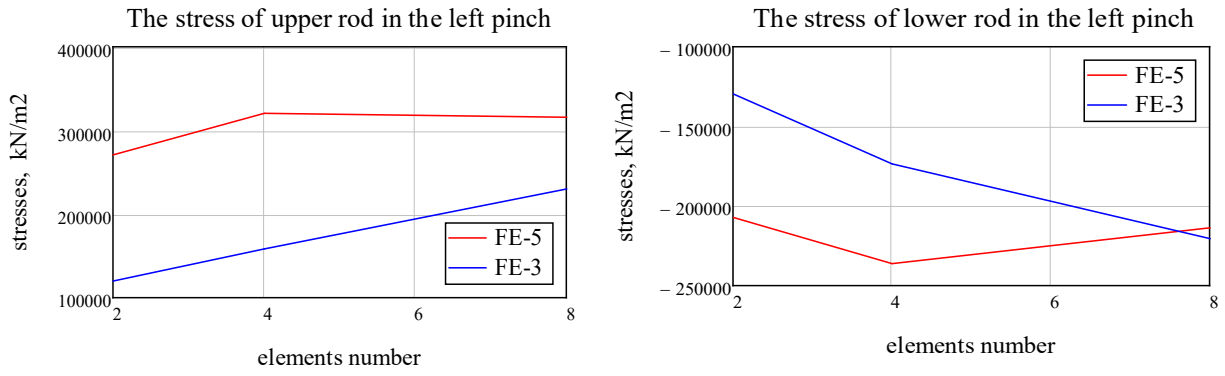

a **b**

Figure 11. The stresses of the reinforcement rods in the left pinch.

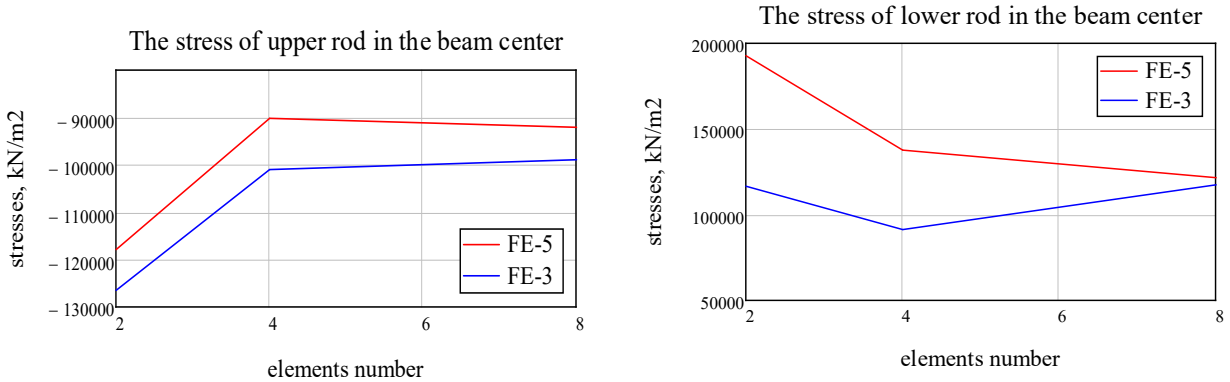

a **b**

Figure 12. The stresses of the reinforcement rods in the beam center.

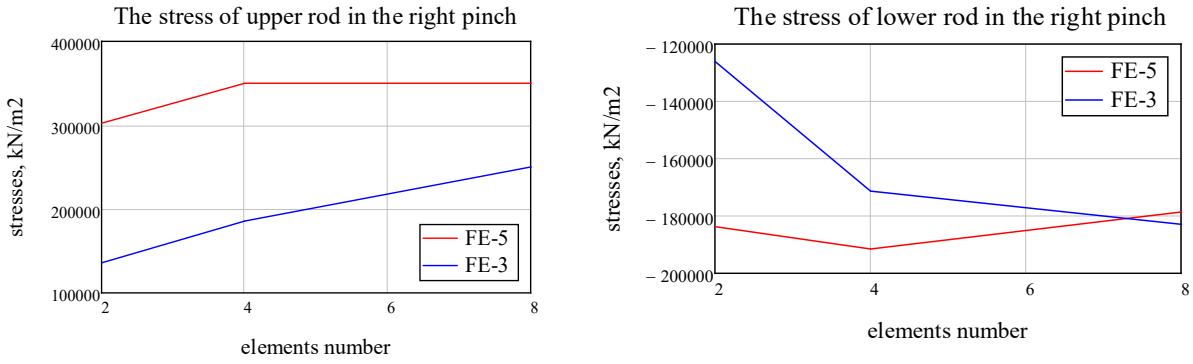

a **b**

Figure 13. The stresses of the reinforcement rods in the right pinch.

***Table 6. The upper reinforcing bars stresses of the support sections,* kN/m^2.**

Number of finite elements	The upper rod stress of the left pinch, kN/m^2			The upper rod stress of the right pinch, kN/m^2		
	FE-3	FE-5	Difference, %	FE-3	FE-5	Difference, %
2	119800	270700	55.7	135900	302400	55.1
4	158300	320400	50.6	185700	350000	46.9
8	230000	315700	27.1	250300	350000	28.5
16	280400	312665	10.3	313085	350000	10.5
32	297195	311805	4.7	337185	350000	3.7

Table 6 shows the tensile reinforcing bars stress values of support sections for various finite elements numbers. The values given in Table 6 show that to obtain a reasonably accurate value we must use four FE-5 or 32 FE-3. Obviously, the differences in stress are determined by the inaccuracy of calculating curvature and longitudinal strain when we use FE-3. FE-5 allows you to calculate more accurately strains of reinforcement and concrete, which is necessary to determine the level of load leading to failure. The stress values of the stretched reinforcement on the support and, therefore, the deformations obtained when we use FE-3 are less than the corresponding stresses calculated when we use FE-5. Therefore, the solution obtained on the basis of FE-3 will determine overestimated failure load values, which will be shown below.

The comparative inclined beam (Fig. 4b) calculations were performed with a gradual load increasing until the tensile reinforcement had reached the yield strength at the support and span sections. The beam was divided into 8 finite elements.

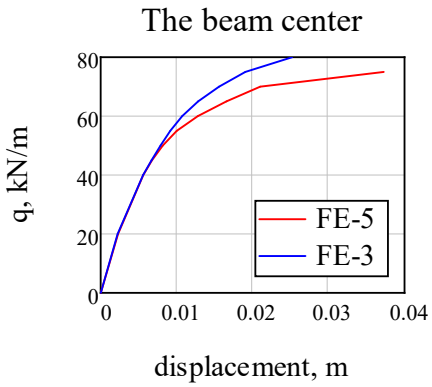

Figure 14. The vertical displacement of inclined beam center.

Fig. 14 shows the vertical displacement changes graph of the beam middle with load increasing. As is known, the system displacements obtained on the Lagrange functional basis when the mesh is refined tends to exact values from below. The approximation to exact values is achieved by increasing the total degrees of freedom number. FE-5 has a greater degrees of freedom number of the nodes compared to the FE-3, therefore, with the same finite element mesh, it gives a more pliable and closer to accurate solution. In addition, the ultimate load obtained using FE-5 is q_z = 75 kN/m, and that obtained using FE-3 is

q_z = 80 kN/m. The ultimate loads differ by about 7 %, and the displacements at the ultimate load differ by 30 %.

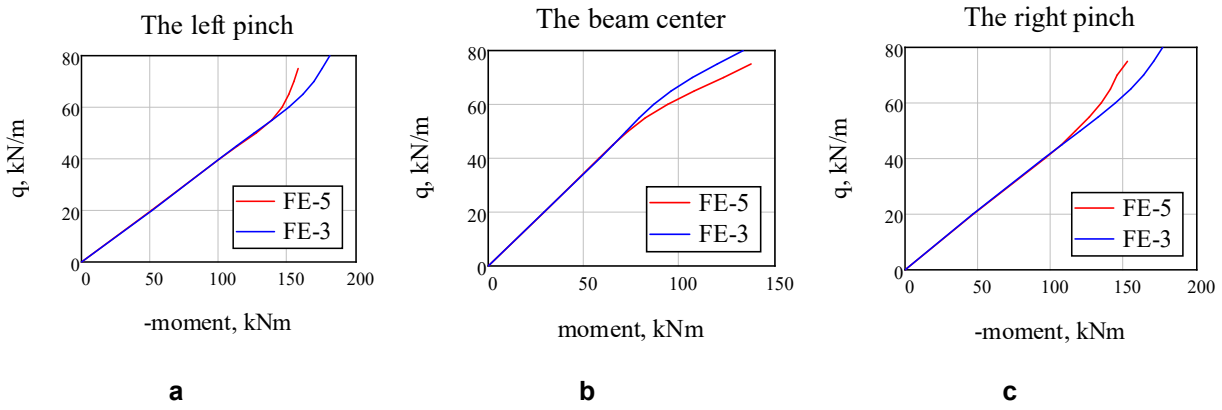

a **b** **c**

Figure 15. The moments in the inclined beam (Fig. 4b).

The bending moments of support sections that arise after the tensile reinforcement yielding onset when we calculated with FE-5 were less than the corresponding moments obtained when we used FE-3 (Fig. 15). Accordingly, the midspan bending moments (Fig. 15b) for FE-5 were larger than those for FE-3. Thus, after the plastic deformations formation, the bending moments' distribution along the beam length becomes different for the two finite elements types, in contrast to the elastic stage of the deformations.

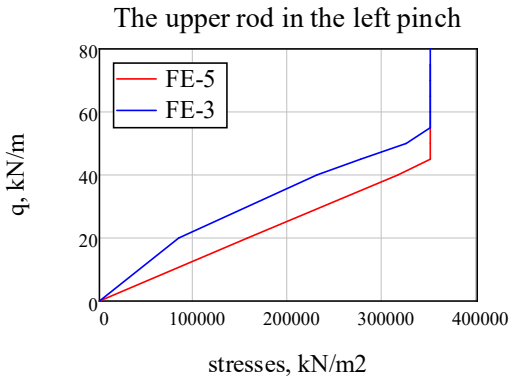

Figure 16. The stress of the upper rod in the left pinch.

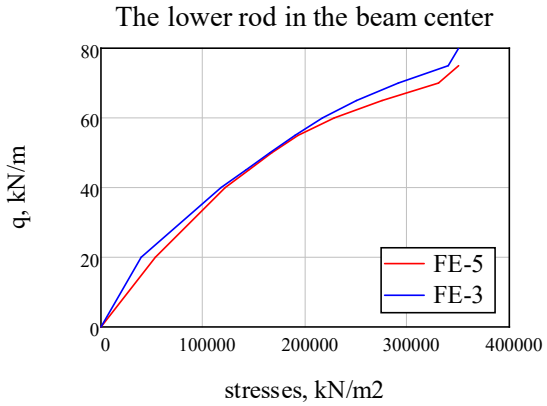

Figure 17. The stress of the lower rod in the beam center.

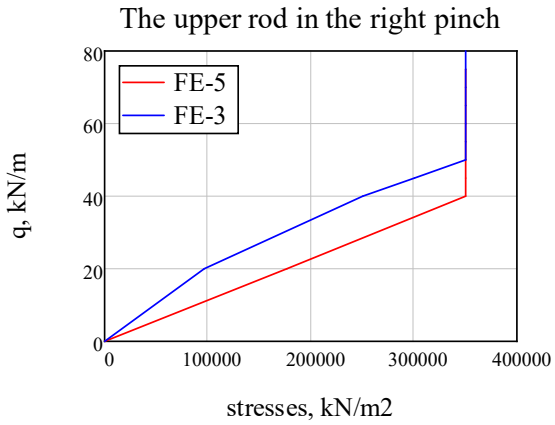

Figure 18. The stress of the upper rod in the right pinch.

Figs. 16–18 show the tensile reinforcement stresses change of the support sections and span middle with an increase of the distributed load to the maximum level. At the same load level, the reinforcing bars stresses of the reference section obtained using FE-5 are greater than the corresponding stresses calculated using FE-3. For example, under load the stresses difference was 21 %. Note that, accordingly, the tensile reinforcement plastic deformations for FE-5 began at a lower load.

4. Conclusions

1. When performing linear calculations, the bending moments, longitudinal forces and displacements do not depend on the number of FE-5 into which the clamped beam is divided. Only one element can be used. For any mesh, the nodal displacements when using FE-3 are calculated accurately, and the intermediate points displacements between nodes approach the exact ones when the mesh is refined. Using FE-5, due to additional degrees of freedom, leads to the displacement's, axis curvature and deformations refinements of the intermediate sections between the finite element nodes.
2. When solving physically nonlinear problems with refinement of the finite element mesh, the solutions obtained for FE-3 tend to the solutions obtained for FE-5. The greatest difference between the two solutions was observed for the longitudinal forces' magnitudes. To calculate more accurately longitudinal forces using FE-3, a mesh of at least eight elements was required. Unlike the linear calculation, there was no coincidence of bending moments and displacements at nodal points obtained using finite elements FE-5 and FE-3.
3. FE-5 allows more accurate calculation of deformations of the reinforcement and concrete, especially at the extreme points, which is necessary to determine the load level leading to failure. The stretched reinforcement stress values on the support and, therefore, the deformations when we used FE-3 were less than the corresponding stresses for FE-5. Therefore, the solution obtained on the basis of FE-3 will determine overestimated breaking load values.
4. The proposed beam finite element with five nodal degrees of freedom makes it possible to determine more accurately the axis curvatures and deformations, which is especially important when solving physically nonlinear problems.

References

1. Akhazhanov, S.B., Vatin, N.I., Akhmediyev, S., Akhazhanov, T., Khabidolda, O., Nurgoziyeva, A. Beam on a two-parameter elastic foundation: Simplified finite element model. Magazine of Civil Engineering. 2023. 121 (5). Article no. 12107. DOI: 10.34910/MCE.121.7
2. Apedo, K.L., Ronel, S., Jacquelin, E., Bennani, A., Massenzio, M. Nonlinear finite element analysis of inflatable beams made from orthotropic woven fabric. International Journal of Solids and Structures. 2010. 47 (16). Pp. 2017–2033. DOI: 10.1016/j.ijsolstr.2010.03.030
3. Arizou, R., Mohareb, M. Finite element formulation for distortional lateral buckling of I-beams. Engineering Structures. 2022. 262. Article no. 114265. DOI: 10.1016/j.engstruct.2022.114265
4. Basso Trujillo, P., Lagier, F., Jolin, M., Massicotte, B., Bissonnette, B. Finite element model of beam-end specimen with different qualities of reinforcing bar encapsulation. Engineering Structures. 2022. 269. Article no. 114789. DOI: 10.1016/j.engstruct.2022.114789
5. Zhu, S., Zhang, Y.X., Lee, C.K. A new finite element procedure for simulation of flexural fatigue behaviours of hybrid engineered cementitious composite beams. Engineering Structures. 2022. 269. Article no. 114839. DOI: 10.1016/j.engstruct.2022.114839

6. Bozorgmehri, B., Obrezkov, L.P., Harish, A.B., Mikkola, A., Matikainen, M.K. A contact description for continuum beams with deformable arbitrary cross-section. Finite Elements in Analysis and Design. 2023. 214. Article no. 103863. DOI: 10.1016/j.finel.2022.103863
7. Fortuna, B., Turk, G., Schnabl, S. A new locking-free finite element for N-layer composite beams with interlayer slips and finger joints. Finite Elements in Analysis and Design. 2023. 220. Article no. 103936. DOI: 10.1016/j.finel.2023.103936
8. Capdevielle, S., Grange, S., Dufour, F., Desprez, C. A shear warping kinematic enhancement for fiber beam elements with a damaging cross-section. Finite Elements in Analysis and Design. 2021. 195. Article no. 103559. DOI: 10.1016/j.finel.2021.103559
9. Čas, B., Saje, M., Planinc, I. Non-linear finite element analysis of composite planar frames with an interlayer slip. Computers & Structures. 2004. 82 (23–26). Pp. 1901–1912. DOI: 10.1016/j.compstruc.2004.03.070
10. Guo, A., Sun, Z., Satyavolu, J. Experimental and finite element analysis on flexural behavior of mortar beams with chemically modified kenaf fibers. Construction and Building Materials. 2021. 292. Article no. 123449. DOI: 10.1016/j.conbuildmat.2021.123449
11. Liao, Q., Yu, J.T., Su, Y.R., Yu, K.Q. Shear failure mechanism and parametric study for seawater sea-sand engineered cementitious composites beams reinforced by FRP bars: Finite element analysis. Construction and Building Materials. 2023. 407. Article no. 133497. DOI: 10.1016/j.conbuildmat.2023.133497
12. Lin, Y., Yan, J., Wang, Z., Zou, C. Experimental study, finite element simulation and theoretical analysis on failure mechanism of steel-concrete-steel (SCS) composite deep beams with UHPC. Engineering Structures. 2023. 286. Article no. 116124. DOI: 10.1016/j.engstruct.2023.116124
13. Nuguzhinov, Zh., Vatin, N., Bakirov, Zh., Khabidolda, O., Zholmagambetov, S., Kurokhtina, I. Stress-strain state of bending reinforced beams with cracks. Magazine of Civil Engineering. 2020. 97 (5). Article no. 9701. DOI: 10.18720/MCE.97.1
14. Kamiński, M., Supeł, Ł. Elastic critical moment for bisymmetric steel profiles and its sensitivity by the finite difference method. International Journal of Applied Mechanics and Engineering. 2016. 21 (1). Pp. 37–59. DOI: 10.1515/ijame-2016-0003
15. Mostafa, A.A.B., Razaqpur, A.G. Finite element model for predicting post delamination behaviour in FRP-retrofitted beams in flexure. Construction and Building Materials. 2017. 131. Pp. 195–204. DOI: 10.1016/j.conbuildmat.2016.11.066
16. Li, X., Li, L., Zhou, M., Wan, S., Chen, J., Kang, A. Refined beam finite element model for thin-walled multi-cell box girders considering distortion and secondary distortional moment deformation effect. Engineering Structures. 2024. 298. Article no. 117042. DOI: 10.1016/j.engstruct.2023.117042
17. Li, X., Wan, S., Zhang, Y., Zhou, M., Mo, Y. Beam finite element for thin-walled box girders considering shear lag and shear deformation effects. Engineering Structures. 2021. 233. Article no. 111867. DOI: 10.1016/j.engstruct.2021.111867
18. Zhu, L., Su, R.K.-L., Li, M.J. Finite beam element with 26 DOFs for curved composite box girders considering constrained torsion, distortion, shear lag and biaxial slip. Engineering Structures. 2021. 232. Article no. 111797. DOI: 10.1016/j.engstruct.2020.111797
19. Lolić, D., Zupan, D., Brojan, M. A consistent finite element formulation for laminated composites with nonlinear interlaminar constitutive law. Composite Structures. 2020. 247. Article no. 112445. DOI: 10.1016/j.compstruct.2020.112445
20. Harish, A.B., Matikainen, M.K. Alleviation techniques for volumetric locking in elements based on the absolute nodal coordinate formulation. Finite Elements in Analysis and Design. 2023. 224. Article no. 103990. DOI: 10.1016/j.finel.2023.103990
21. Hoffmeyer, D., Damanpack, A.R. Bending and torsion induced stresses in cylindrically orthotropic and inhomogeneous timber beams. Finite Elements in Analysis and Design. 2024. 229. Article no. 104072. DOI: 10.1016/j.finel.2023.104072
22. Hu, Y.J., Liu, M., Zhu, W., Jiang, C. An adaptive differential quadrature element method for large deformation contact problems involving curved beams with a finite number of contact points. International Journal of Solids and Structures. 2017. 115–116. Pp. 200–207. DOI: 10.1016/j.ijsolstr.2017.03.020
23. Lalin, V.V., Dmitriev, A.N., Diakov, S.F. Nonlinear deformation and stability of geometrically exact elastic arches. Magazine of Civil Engineering. 2019. 89 (5). Pp. 39–51. DOI: 10.18720/MCE.89.4
24. Murin, J., Aminbaghai, M., Hrabovsky, J., Gogola, R., Kugler, S. Beam finite element for modal analysis of FGM structures. Engineering Structures. 2016. 121. Pp. 1–18. DOI: 10.1016/j.engstruct.2016.04.042
25. Santos, H.A.F.A., Silberschmidt, V.V. Hybrid equilibrium finite element formulation for composite beams with partial interaction. Composite Structures. 2014. 108. Pp. 646–656. DOI: 10.1016/j.compstruct.2013.09.062
26. Schnabl, S., Saje, M., Turk, G., Planinc, I. Locking-free two-layer Timoshenko beam element with interlayer slip. Finite Elements in Analysis and Design. 2007. 43 (9). Pp. 705–714. DOI: 10.1016/j.finel.2007.03.002
27. Skrinar, M. Computational analysis of multi-stepped beams and beams with linearly-varying heights implementing closed-form finite element formulation for multi-cracked beam elements. International Journal of Solids and Structures. 2013. 50 (14–15). Pp. 2527–2541. DOI: 10.1016/j.ijsolstr.2013.04.005
28. Rybakov, V.A., Lalin, V.V., Ivanov, S.S., Azarov, A.A. Coordinate functions quadratic approximation in V.I. Slivker's semi-shear stability theory. Magazine of Civil Engineering. 2019. 89 (5). Pp. 115–128. DOI: 10.18720/MCE.89.10
29. Tyukalov, Yu.Ya. Calculation of circular plates with assuming shear deformations. IOP Conference Series: Materials Science and Engineering. 2019. 687 (3). Article no. 033004. DOI: 10.1088/1757-899X/687/3/033004
30. Tyukalov, Yu.Ya. Method of plates stability analysis based on the moments approximations. Magazine of Civil Engineering. 2020. 95 (3). Pp. 90–103. DOI: 10.18720/MCE.95.9
31. Tyukalov, Yu.Ya. Arbitrary quadrangular finite element for plates with shear deformations. Magazine of Civil Engineering. 2021. 107 (7). Article no. 10707. DOI: 10.34910/MCE.107.7
32. Tyukalov, Yu.Ya. Refined finite element of rods for stability calculation. Magazine of Civil Engineering. 2018. 79 (3). Pp. 54–65. DOI: 10.18720/MCE.79.6
33. Walls, R., Viljoen, C., de Clercq, H. A nonlinear, beam finite element with variable, eccentric neutral axis. Engineering Structures. 2019. 187. Pp. 341–351. DOI: 10.1016/j.engstruct.2019.02.056
34. Zhao, Y., Yuan, Y., Wang, C.L., Meng, S. Experimental and finite element analysis of flexural performance of steel-timber composite beams connected by hybrid-anchored screws. Engineering Structures. 2023. 292. Article No. 116503. DOI: 10.1016/j.engstruct.2023.116503

35. Zhang, X., Li, Z. Shear behaviour of stiffened hollow glulam beams: Experiments, analytical model, and finite element analysis. Construction and Building Materials. 2023. 392. Article Nno. 131826. DOI: 10.1016/j.conbuildmat.2023.131826
36. Zhang, X., Luo, L., Xie, X., Zhang, Y., Li, Z. Flexural bearing capacity and stiffness of stiffened hollow glulam beams: Experiments, finite element analysis and calculation theory. Construction and Building Materials. 2022. 345. Article no. 128407. DOI: 10.1016/j.conbuildmat.2022.128407
37. Gallagher, R.H. Finite element analysis: fundamentals. N.J.: Englewood Cliffs, 1975. 416 p.

Contacts:

Yury Tyukalov, *Doctor of Technical Sciences*
ORCID: https://orcid.org/0000-0001-6184-2365
E-mail: yutvgu@mail.ru

Received 23.11.2023. Approved after reviewing 11.06.2024. Accepted 11.06.2024.